Electronic Supplementary Materials

For https://doi.org/10.1631/jzus.A2100584

Free-standing MXene/chitosan/Cu_2O electrode: an enzyme-free and efficient biosensor for simultaneous determination of glucose and cholesterol

Tao HU[1,2], Man ZHANG[1,2], Hui DONG[1,2], Tong LI[1,2], Xiao-bei ZANG[3], Xiao LI[1,2], Zhong-hua NI[1,2]

[1]*School of Mechanical Engineering, Southeast University, Nanjing 211189, China*
[2]*Jiangsu Key Laboratory for Design and Manufacture of Micro-Nano Biomedical Instruments, Southeast University, Nanjing 211189, China*
[3]*School of Materials Science and Engineering, China University of Petroleum (East China), Qingdao 266580, China*

This file contains:

S1: Reagents and chemicals

Sodium hydroxide (NaOH) was obtained from Sinopharm group chemical reagent Co., Ltd. Cu-pric acetate ($Cu(CH_3COO)_2$) was bought from Beijing HWRK chemical Co. Ltd. Titanium alu-minum carbide of 400 mesh (Ti_3AlC_2) was received from Jilin 11 technology Co., Ltd. Cholesterol was purchased from Shanghai Aladdin biochemical Co., Ltd. Lithium fluoride (LiF) was purchased from Shanghai Macklin biochemical Co., Ltd. Glucose was obtained from Shanghai Sigma Al-drich trading Co., Ltd. Ascorbic acid (AA) was purchased from Shanghai Alfa Aesar chemical Co., Ltd. All other reagents were brought from Sigma with guaranteed reagent (GR) level. The experi-ments were conducted with double- distilled water (ultra-pure conductivity of ≥ 18.25 MΩ).

S2: Instrumentation and measurements

Surface morphology was conducted by SEM (FEI Quanta 200 microscope) and corresponding energy dispersive X-ray spectroscopy (EDS). TEM was performed on a FEI Tecnai G2 T20 microscope with 200 kV operation voltage. PHI 5000 VersaProbe and Ultima IV were performed for XPS and XRD analysis, respectively. Zeta-potential was conducted under 90plus (Brookhaven instrument Corp.). Electrochemical experiments (CV) were performed with a CHI 660D electrochemical workstation, bought from Shanghai CH Instrument Company, China. Membrane Celgard 3501 was obtained from Jilin 11 technology Co., Ltd. During the measurements, a three-electrode configuration was conducted with a modified self-assembled film as the working electrode, Ag/AgCl (3 M KCl saturated) as the reference electrode, and platinum sheet as the counter electrode. 60 mL sodium hydroxide (NaOH) was selected as the electrolyte. Cholesterol detection was achieved by dissolving in ethanol, followed by dilution in NaOH as per requirement for a given concentration.

S3: Preparation of 2D Ti_3C_2 Mxene

Ti_3C_2 MXene was obtained by selectively etching of Al from the ternary layered Ti_3AlC_2 (Scheme 1). 2 g LiF was added to 40 mL 9 M HCl aqueous solution under magnetic stirring, followed by slowly adding 2 g Ti_3AlC_2 in 10 min. The mixture was transferred to a 35 °C water bath, treated for 24 h, and then centrifuged and washed with deionized water until the pH>6. Subsequently, the dispersion was under sonication and centrifugation for 1 h respectively. The supernatant was gathered as an MXene solution and the MXene powder was obtained after freeze-drying of the suspension.

S4: Formation of MXene/CTS film

CTS was dissolved in 3% acetic acid solution reaching a concentration of 0.5%. The 5 mL mixture of MXene and CTS solution (4:1) with opposite charges was incubated in a refrigerator under 4 °C for 12 h for

full electrostatic interaction. The MXene/CTS film with diameter 11 mm was prepared through a simple vacuum-assisted filtration method by a microporous monolayer membrane (Celgard 3501), followed by vacuum drying at 60 °C.

S5: Modification of Cu_2O on MXene/CTS film

Cu_2O was modified on MXene/CTS through a potentiostatic electrodeposition procedure in an 0.05 M $Cu(CH_3COO)_2$ aqueous solution with a three-electrode configuration. The fabricated film was used as the working electrode. The electrodeposition potential was set at -0.4 V, and the time at 2000 s. Finally, the working electrode was washed with ethanol and deionized water, and then dried under air for further characterization.

S6: The morphology of MXene/CTS/Cu_2O

The morphology of the as-synthesized film was characterized by TEM and SEM. The TEM images of the exfoliated MXene reveal single and a few layers of flat sheets (**Figs. S1a and 1b**). The hexagonal lattice characteristics of the MXene nanosheet are shown in the Selected Area Electron Diffraction (SAED) diagram in the inset of Fig. S1a. In addition, Fig. S1b shows a constant interplanar distance of about 1.235 nm, confirming the 2D lamellar structure of the prepared MXene. **Fig. S1c** further depicts the layered structure of multilayer MXene, where the Al layers of MAX were selectively etched away by HCl. The Zeta potentials of MXene and CTS were -20.225 mV and +1.34167 mV, respectively (**Fig. S2a**) and in the XPS spectra of MXene/CTS/Cu_2O (**Fig. S2b**), there was one new small N (1s) peak from CTS, confirming the adsorption of CTS on the MXene surface (Liu et al., 2017). The SEM image of MXene/CTS is shown in **Fig. S1d,** the relatively smooth surface demonstrates the forceful electrostatic interaction of MXene (-) and CTS (+), and the strip projections further confirm the successful mixture of CTS. The dense and homogeneous distributed aggregation of Cu_2O particles on the surface with an average edge length of ~300 nm verifies the modification by electrodeposition (**Fig. S1e**). Moreover, the energy dispersive X-ray spectroscopy (EDS) mapping of MXene/CTS and MXene/CTS/Cu_2O proves the presence of Ti, C, Cu and O elements in the products (**Fig. S3**).

S7: The crystal structure of the MXene/CTS/Cu_2O

XRD is a widely-used technique to investigate the crystal structure of the as-prepared samples. As shown in **Fig. S1f**, the peak of MAX at 40° disappears in MXene/CTS/Cu_2O, confirming the removal of Al layers during etching. The diffraction peaks of Cu_2O with 2θ values at 25° and 36.6° correspond to the crystal plane (110) and (111) of crystalline Cu_2O, respectively (JCPDS 05-0667). The diffraction peak with 2θ values at 5.5° belongs to the (002) plane of Mxene (Naguib et al., 2012) and the smooth peak at 17.5° is attributed to CTS (JCPDS 21-1272). The characteristic diffraction peaks of MXene, CTS and Cu_2O appear to indicate the successful preparation of the MXene/CTS/Cu_2O film, and no diffraction peaks related to impurities are found.

S8: The chemical states and valence of composites of MXene/CTS/Cu_2O nanohybrid

Figs. S1g and 1h show the XPS profiles of MXene/CTS/Cu_2O nanohybrid, which were used to determine the chemical states and valence of composites. In Fig. S1g, the peaks located at the binding energies of around 457.4 eV and 463.5 eV can be assigned to Ti-O 2p3/2 and Ti-O 2p1/2 respectively (Dong et al., 2017). The high resolution XPS spectrum of the Cu 2p core level is displayed in Fig. S1h. The peaks for Cu 2p3/2 and Cu 2p1/2 are located at binding energies of 932.8 eV and 953.5 eV respectively and match well with the reported values of the Cu^{1+} oxidation state of Cu_2O. The presence of satellite peaks indicates the existence of Cu^{2+} along with Cu_2O (Dong et al., 2017; Qin et al., 2016).

S9: Selection for detecting peaks

Figs. S6a and **6c** show CVs of MXene/CTS/Cu_2O at different concentrations of glucose and cholesterol, respectively. Peak I exhibits a linear current response only for cholesterol, and the oxidation currents at the potential of 0.35 V which named as peak VI establishes a greater sensitivity to glucose than peak V. Furthermore, peak IV varies both with glucose and cholesterol addition, which may be caused by the synthetic effect of MXene and Cu_2O. In addition, the current responses of peak III are very faint, which are not sensitive to both glucose and cholesterol. As shown in **Fig. S7** (inner plot), peak II has a poor linear fit with addition of cholesterol. Therefore, peak I and VI were determined for simultaneous sensing of cholesterol and glucose with a significant potential separation. The linear relationship between the concentration and corresponding currents at selected peaks were plotted in **Figs. S6b and 6d**. As observed, the electrocatalytic currents for both glucose and cholesterol are finely linear to their concentration, demonstrating a good application prospect for the all-in-one monitoring of multi-metabolites.

S10: Deduction for cholesterol sensing mechanism

There are literatures supporting that hydroxyl radicals (.OH) can initiate the cholesterol auto-oxidation to produce oxysterols (Khaliq et al., 2020; Lee et al., 1997). The Equation 4 was carefully deduced through the analysis of experimental phenomena and comparative experiments. Firstly, by observing the CV plots, the peakI current response (Cu^{1+} to Cu) decreases with cholesterol addition, and there is no response to glucose, which proves that Cu^{1+} participates in the catalytic reaction for cholesterol. Secondly, there was no current response in a neutral PBS solution, which proved that OH^- are essential for reaction. As shown in **Fig. S8**, after a long period of testing, Cu^{1+} was gradually consumed, which convinced the deduced mechanism.

S11: Supporting figures: Figs. S1–S10

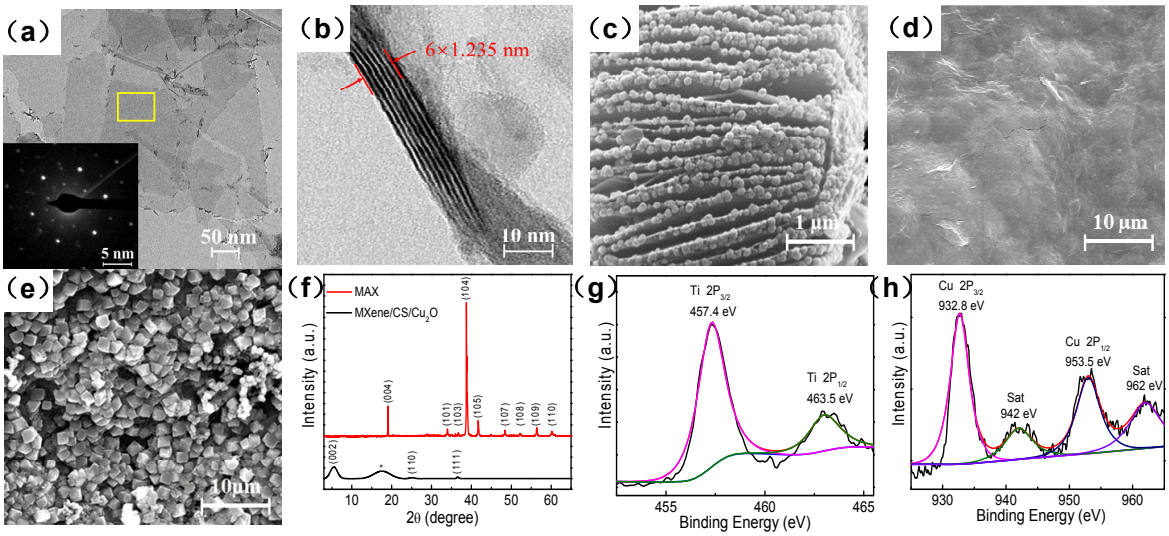

Fig. S1. TEM images of (a) and (b) exfoliated MXene sheets. The inset in (a) shows the selected area electron diffraction pattern from the region marked with a yellow box. SEM images of (c) MXene; (d) MXene/CTS; (e) MXene/CTS/Cu2O. XRD patterns of MAX powders and MXene/CTS/Cu2O film (f). High resolution XPS spectra of MXene/CTS/Cu_2O: (g) Ti 2p, (h) Cu 2p.

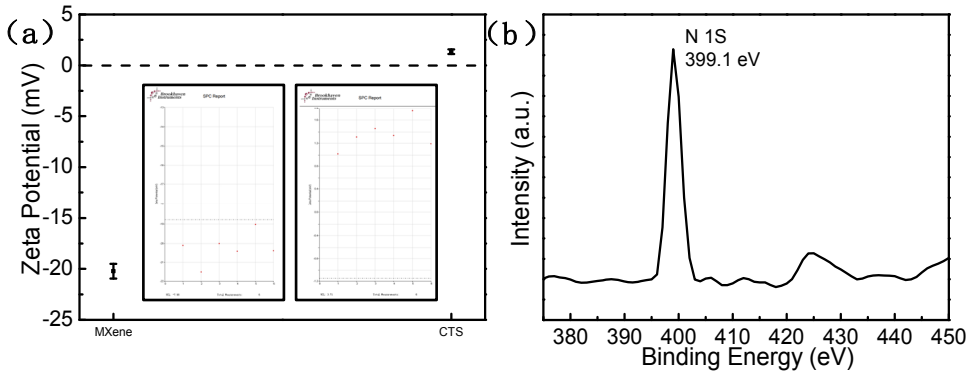

Fig. S2. (a): Zeta potential of the fabricated MXene and CTS (0.5wt.%); (b): XPS spectra of Mxene/CTS/Cu_2O : N 1s.

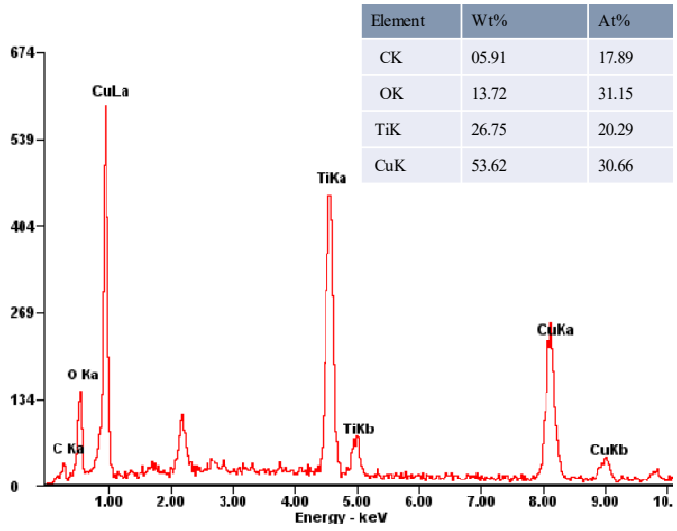

Fig. S3. EDS mapping of the MXene/CTS/Cu_2O.

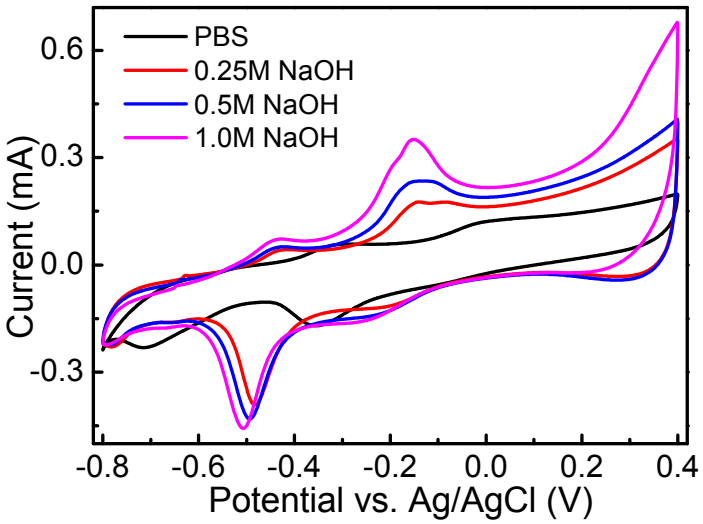

Fig. S4. CV behaviors of MXene/CTS/Cu_2O biosensor in PBS and 0.25 M, 0.5 M and 1.0 M NaOH electrolyte.

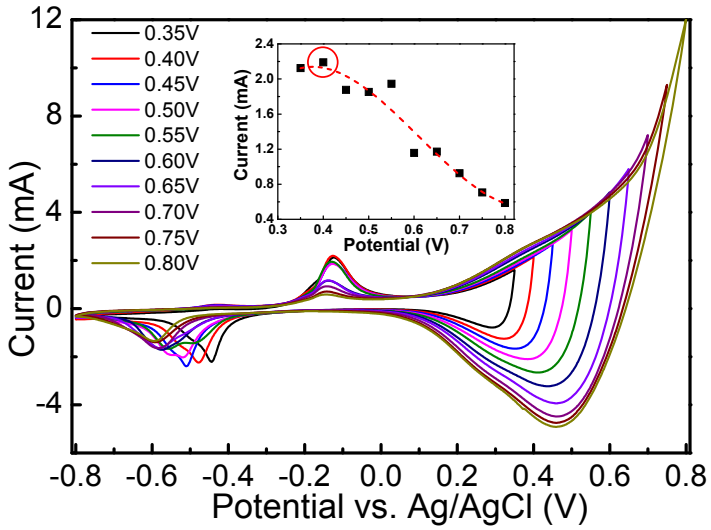

Fig. S5. CV behaviors of MXene/CTS/Cu_2O electrode in 1.0 M NaOH at the range from -0.8 V to 0.35 V, 0.4 V, 0.45 V, 0.50 V, 0.55 V, 0.60 V, 0.65 V, 0.70 V, 0.75 V, 0.8 V. The innet plot is the potential *vs.* peak current value at -0.15 V.

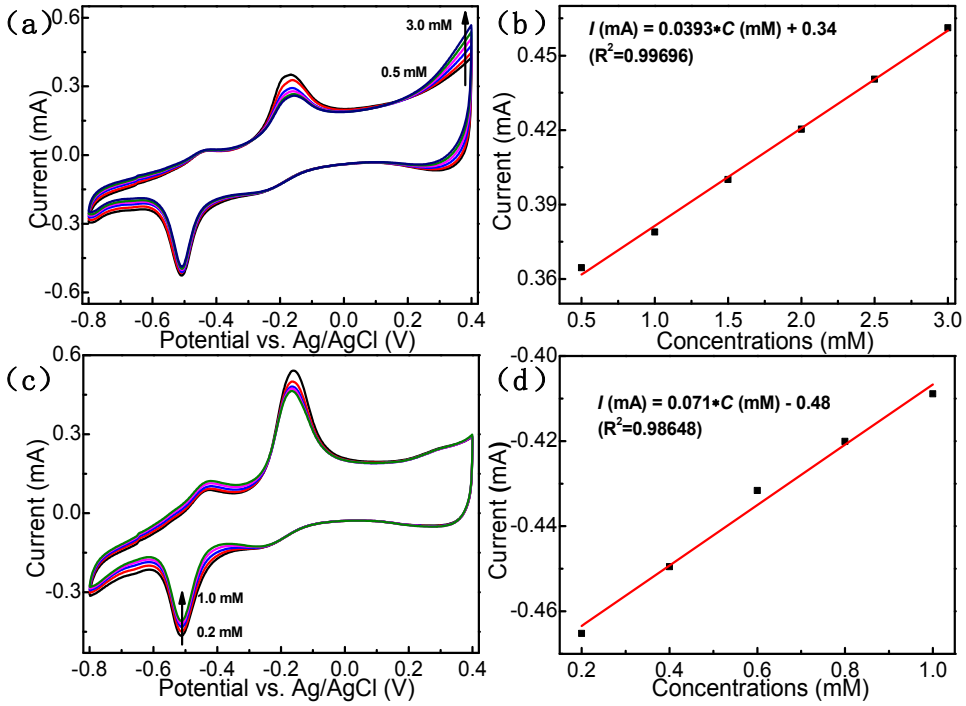

Fig. S6. CV responses of MXene/CTS/Cu_2O towards (a) glucose from 0.5 mM to 3.0 mM and (c) cholesterol from 0.2 mM to 1.0 mM with corresponding fitting curves in (b) and (d).

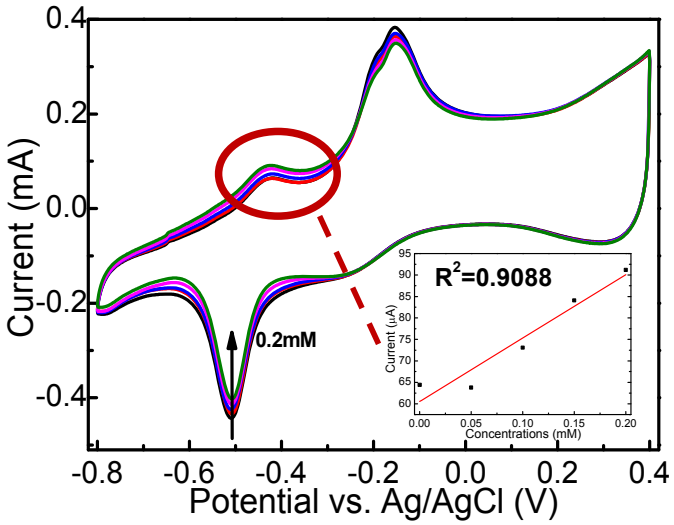

Fig. S7. CV curves of MXene/CTS/Cu_2O with 1mM glucose towards cholesterol sensing (cholesterol: from 0 mM to 0.2 mM at 0.05 mM interval); Plotted relationship curve of MXene/CTS/Cu_2O between electrocatalytic current and cholesterol concentration at peak II.

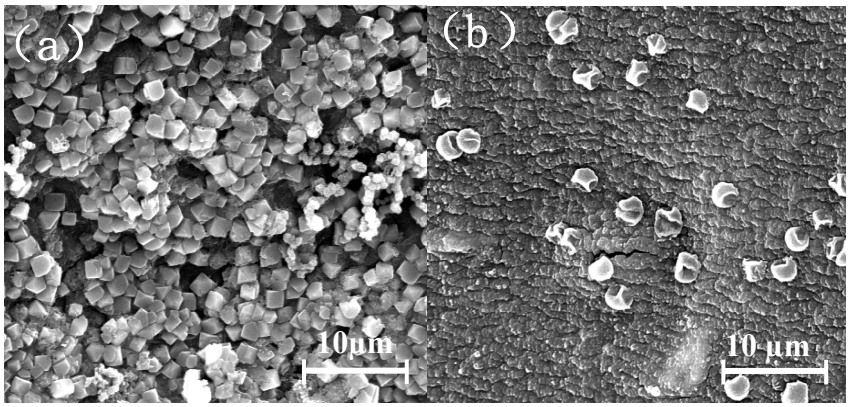

Fig. S8. SEM images of MXene/CTS/Cu_2O before (a) and after (b) tests

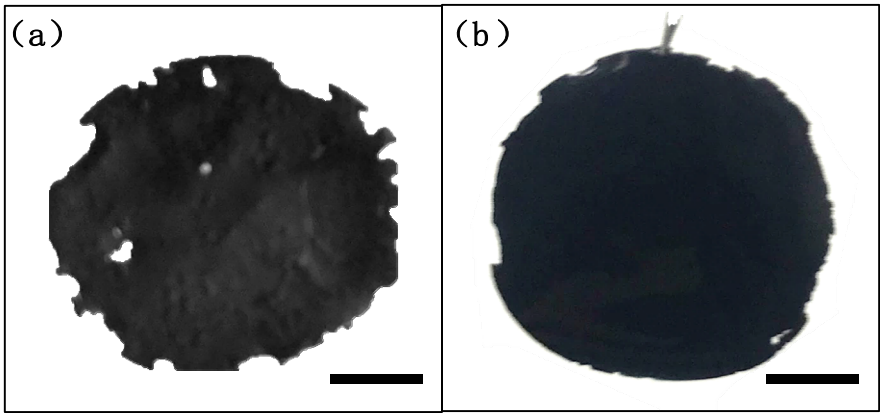

Fig. S9. MXene films after 10 minutes of ultrasound treatment without (a) and with CTS mixed (b). Scale bars: 3 mm.

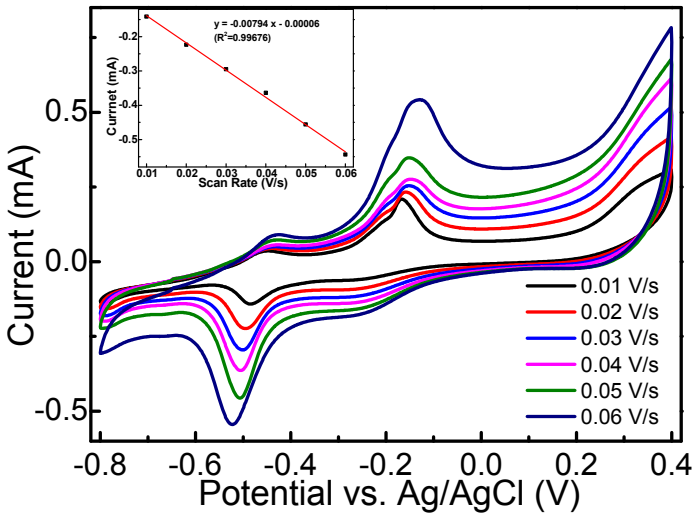

Fig. S10. CV responses of MXene/CTS/Cu_2O electrode in 1.0 M NaOH at different scan rates from 0.01 V/s to 0.06 V/s.

S12: Supporting table: Table S1.

Table S1 Electrochemical performances comparison of MXene/CTS/Cu_2O for glucose and cholesterol detection with other modified electrodes based on nanomaterial and polymer.

Modified electrode	Metabolites	Sensitivity ($\mu A.mM^{-1}.cm^{-2}$)	Linear Range (uM)	LOD (uM)	Enzymes modified	Reference
Co@MoS_2/CNTs/GCE	Glucose	131.69	Not Provided - 5200	0.08	-	(Li et al., 2019)
NC-NiS@NS-NiS	Glucose	54.60	20 - 5000	0.0083	-	(Arivazhagan et al., 2021)
BPCNF/GCE	Glucose	123.28	0.2 - 100	0.023	GO_x	(Liang et al., 2019)
Cu_2O NPs/TNTs	Cholesterol	6034.04	24.4 - 622	0.05	-	(Khaliq et al., 2020)
Pt-NC/SPCE	Cholesterol	132	2 - 486	2	ChO_x	(Eom et al., 2020)
PPI/QDs/GCE	Cholesterol	111.16	100 - 10000	75	ChO_x	(Mokwebo et al., 2018)
Pt/rGO/P_3ABA/SPCE	Glucose /Cholesterol	22.01 / 15.94	250 – 6000 /250 - 4000	44.3 /40.5	GO_x/ChO_x	(Phetsang et al., 2019)
CuO-NPs/GCE	Glucose /Cholesterol	1098.37 / Not Provided	5 – 600 / 1 - 15	0.59 / 0.43	-/ChO_x	(Wu et al., 2019)
MXene/CTS/ Cu_2O	**Glucose/ Cholesterol**	**60.295 / 215.71**	**52.4– 2000 /49.8 - 200**	**52.4 / 49.8**	**-**	**This work**

Reference

Arivazhagan M, Santhosh YM, Maduraiveeran G, 2021. Non-Enzymatic Glucose Detection Based on NiS Nanoclusters@NiS Nanosphere in Human Serum and Urine. *Micromachines* 12(4). https://doi.org/10.3390/mi12040403

Dong K, He J, Liu J, et al., 2017. Photocatalytic performance of Cu_2O-loaded TiO_2/rGO nanoheterojunctions obtained by UV reduction. *J Mater Sci* **52**(11): 6754-6766. https://doi.org/10.1007/s10853-017-0911-2

Eom KS, Lee YJ, Seo HW, et al., 2020. Sensitive and non-invasive cholesterol determination in saliva via optimization of enzyme loading and platinum nano-cluster composition. *Analyst* **145**(3): 908-916. https://doi.org/10.1039/c9an01679a

Khaliq N, Rasheed MA, Cha G, et al., 2020. Development of non-enzymatic cholesterol bio-sensor based on TiO_2 nanotubes decorated with Cu_2O nanoparticles. Sensors and Actuators B: Chemical 302: 127200. https://doi.org/10.1016/j.snb.2019.127200

Lee, J.H., D.W. Shoeman, S.S. Kim, et al., 1997. The effect of superoxide anion in the production of seven major cholesterol oxidation products in aptoric and protic conditions. International Journal of Food Sciences and Nutrition 48(2): 151-159. https://doi.org/10.3109/09637489709006975

Li X, Ren K, Zhang M, et al., 2019. Cobalt functionalized MoS2/carbon nanotubes scaffold for enzyme-free glucose detection with extremely low detection limit. *Sensors and Actuators B: Chemical* **293**: 122-128. https://doi.org/10.1016/j.snb.2019.04.137

Liang T, Zou L, Guo X, et al., 2019. Rising Mesopores to Realize Direct Electrochemistry of Glucose Oxidase toward Highly Sensitive Detection of Glucose. *Adv Funct Mater* **29**(44): 1903026. https://doi.org/10.1002/adfm.201903026

Liu, W., W. Liu, D. Wei, et al., 2017. Synthesis of N,N-Bis(2-hydroxypropyl)laurylamine and its flotation on quartz. *Chemical Engineering Journal* **309**: 63-69. https://doi.org/10.1016/j.cej.2016.10.036

Mokwebo K, Oluwafemi O, Arotiba O, 2018. An Electrochemical Cholesterol Biosensor Based on A CdTe/CdSe/ZnSe Quantum Dots—Poly (Propylene Imine) Dendrimer Nanocomposite Immobilisation Layer. *Sensors-Basel* **18**(10): 3368. https://doi.org/10.3390/s18103368

Naguib M, Mashtalir O, Carle J, et al., 2012. Two-Dimensional Transition Metal Carbides. *Acs Nano* **6**(2): 1322-1331. https://doi.org/10.1021/nn204153h

Phetsang S, Jakmunee J, Mungkornasawakul P, et al., 2019. Sensitive amperometric biosensors for detection of glucose and cholesterol using a platinum/reduced graphene oxide/poly(3-aminobenzoic acid) film-modified screen-printed carbon electrode. *Bioelectrochemistry* **127**: 125-135. https://doi.org/10.1016/j.bioelechem.2019.01.008

Qin Y, Zhang J, Wang Y, et al., 2016. Supercapacitive performance of electrochemically doped TiO_2 nanotube arrays decorated with Cu_2O nanoparticles. *Rsc Adv* **6**(53): 47669-47675. https://doi.org/10.1039/c6ra08891k

Wu Q, He L, Jiang ZW, et al., 2019. CuO nanoparticles derived from metal-organic gel with excellent electrocatalytic and peroxidase-mimicking activities for glucose and cholesterol detection. *Biosensors and Bioelectronics* **145**: 111704. https://doi.org/10.1016/j.bios.2019.111704